Electrochimica Acta 54 (2009) 7495–7501

Contents lists available at ScienceDirect

Electrochimica Acta

journal homepage: www.elsevier.com/locate/electacta

Raman and ^{29}Si NMR spectroscopic characterization of lanthanum silicate electrolytes: Emphasis on sintering temperature to enhance the oxide-ion conductivity

Seung Hwan Jo [1], P. Muralidharan [1], Do Kyung Kim *

Department of Materials Science and Engineering, Korea Advanced Institute of Science and Technology (KAIST), 335 Gwahak-ro, Yuseong-gu, Daejeon 305-701, Republic of Korea

ARTICLE INFO

Article history:
Received 24 May 2009
Received in revised form 23 July 2009
Accepted 31 July 2009
Available online 11 August 2009

Keywords:
Lanthanum silicate
Apatite-structure
DEA process
Raman spectroscopy
Solid state ^{29}Si NMR
Sintering temperature
Impedance
SOFC

ABSTRACT

Enhancement of oxide-ion conductivity has been investigated with emphasis on the high sintering temperature of apatite-type structure lanthanum silicate ($La_{10}Si_6O_{27}$) as a potential electrolyte for intermediate-temperature solid oxide fuel cells (IT-SOFCs). The influence of the sintering temperatures 1500, 1550, 1600 and 1650 °C as a function of ionic conductivity of the $La_{10}Si_6O_{27}$ electrolyte synthesized via a diethylamine (DEA) precipitation process has been characterized using impedance spectroscopy. The ionic conductivity of the $La_{10}Si_6O_{27}$ electrolyte sintered at 1650 °C revealed a higher value (1.22×10^{-2} S cm^{-1} at 700 °C) of one order of magnitude than the pellets sintered at lower temperatures. The sintered $La_{10}Si_6O_{27}$ pellets have been characterized by ^{29}Si NMR and Raman spectroscopy. The ^{29}Si NMR data showed the characteristic secondary peak at ~81.2 ppm, which confirmed the interstitial oxygen content contributing to high oxide-ion conduction. The Raman spectra revealed the appearance of a new resolved band centered at 861 cm^{-1} for the pellet sintered at 1650 °C compared with lower temperatures sintered pellets. The results confirmed the possibility of local structural distortion to create additional pathways for interstitial oxide-ion conduction between channels leading to higher conductivity for the pellets sintered above 1600 °C. Thus, the conduction pathway may be determined by the co-operative displacements of the SiO_4 substructure units formed at elevated sintering temperatures for high oxide-ion conductivity.

1. Introduction

Development of solid electrolytes with high ionic conductivity to maintain low ohmic loss at reduced operating temperatures is one of the major challenging issues for the commercialization of intermediate-temperature solid oxide fuel cells (IT-SOFCs) [1–4]. In recent years, apatite rare-earth silicates, $RE_{9.33+x}Si_6O_{26+3x/2}$ (RE = La, Nd, Sm, Gd, and Dy), materials have been attracting a considerable interest as the solid electrolytes for IT-SOFCs [5,6]. The significant characteristics of these apatite solid electrolytes are the high oxide-ion conductivity at the reduced operating temperature range and the high oxygen ion transference numbers (>0.9) over a wide range of oxygen partial pressures [5,7–9]. Among many apatite rare-earth silicates, the $La_{10}Si_6O_{27}$ composition exhibits the highest oxide-ion conductivity (4×10^{-3} S cm^{-1} at 500 °C) [5].

However, the main limitation encountered by the lanthanum silicates is the difficulty to prepare samples with the pure single-phase and high densification below 1700 °C. In the literature, there are many reports that claim for the development of better synthesis methods to achieve high densification at reduced sintering temperatures. Recently, Jo et al. [10], Tao and Irvine [11] and Tian et al. [12] reported the synthesis of lanthanum silicate nanopowders through wet chemical methods, such as a precipitation and a sol–gel route. The apatites synthesized by those methods provided significant improvement on phase formation at lower calcination temperatures and good densification at reduced sintering temperatures below 1500 °C. On the other hand, their ionic conductivities were almost one order of magnitude lower compared with apatites sintered at higher temperature above 1600 °C.

In the apatite-type structured lanthanum silicate electrolytes, oxide-ions are believed to migrate via an interstitial conduction mechanism, in which the interstitial oxygen ions passing through cavities located between La channels and isolated SiO_4 tetrahedra along the *c*-axis [13–16]. Recently, solid state ^{29}Si NMR studies of apatite-type silicates have confirmed the presence of interstitial oxygen sites, which is correlated with the Si environment

* Corresponding author. Tel.: +82 42 350 4118; fax: +82 42 350 3310.
E-mail address: dkkim@kaist.ac.kr (D.K. Kim).
[1] Equal contribution of work.

0013-4686/$ – see front matter © 2009 Elsevier Ltd. All rights reserved.
doi:10.1016/j.electacta.2009.07.086

and the ionic conductivity. It has been suggested that the presence of different Si environments is attributed to the SiO_4 unit adjacent to an interstitial oxide-ion [17,18]. Following the important spectroscopic results from the literature, the present study intends to investigate in detail the influence of the sintering temperatures related to the local structural distortion and the defect non-stoichiometry on the ionic conductivity of the lanthanum silicates electrolytes. The study is supported with characterization techniques.

In this study, $La_{10}Si_6O_{27}$ electrolytes were sintered at 1500, 1550, 1600 and 1650 °C using a diethylamine precipitation process synthesized nanopowders. The ionic conductivities of the different temperatures sintered pellets were characterized by impedance spectroscopy. The origin of difference in ionic conductivity for the different temperatures sintered pellets was characterized by Raman spectroscopy to describe the structural distortion of the SiO_4 tetrahedra units and ^{29}Si NMR spectroscopy to identify the interstitial oxide-ions conduction mechanism.

2. Experimental

Apatite $La_{10}Si_6O_{27}$ nanopowder was synthesized based on the detailed procedure described in our previous reports [10,19]. The DEA (diethylamine) was used as a precipitant in the precipitation method to produce ultrafine particles. The powders were calcined at 800 and 1400 °C for 4 h, separately, and ball-milled for 24 h in ethanol using zirconia media. After subsequent drying and granulation, the powders were uniaxially pressed with a cylindrical stainless mold, followed by cold isostatic pressure under 200 MPa. The $La_{10}Si_6O_{27}$ pellets were sintered in an electric furnace at 1500, 1550 °C for 4 h and 1600, 1650 °C for 2 h in air, with a heating ramp of 5 °C min^{-1}. The pellets were sintered at 1500 °C (LS1500) and 1550 °C (LS1550) using the powder calcined at 800 °C (LS800). The powder calcined at 1400 °C was used for the pellets sintered at 1600 °C (LS1600) and 1650 °C (LS1650).

The synthesized samples were characterized using an X-ray diffractometer (D/MAX-IIIC X-ray diffractometer, Rigaku, Tokyo, Japan), Cu K_α radiation (λ = 0.15406 nm at 40 kV and 45 mA). The XRD patterns were recorded for the calcined powders and the fine ground powders of the pellets sintered from 1500 to 1650 °C at a scan rate of 3 min^{-1}. The relative density of the pellets under different sintering conditions was measured by the Archimedes method in DI water as an intrusion medium. The densification and grain morphology of the sintered pellets were characterized by a scanning electron microscope (FE-SEM Philips XL30 FEG, Eindhoven, Netherland).

For impedance analysis, the surfaces of the sintered pellets were polished. Platinum paint was then applied to either side of the pellets, which were then heat-treated at 1000 °C for 1 h to facilitate stable contact of the electrode to the pellet surfaces. The platinum electrode-coated pellet was then attached to a platinum mesh, which was connected with platinum wires and sandwiched in a spring-loaded specimen holder. The electrical conductivity of the pellets was studied in the presence of air by alternating current (ac) impedance spectroscopy (Solartron 1260 impedance/Gain-phase analyzer, Farnborough, UK), which was interfaced with a computer-controlled program for data acquisition. The impedance spectra were measured over a frequency range of 1 Hz–10 MHz as a function of temperature from 350 to 700 °C.

^{29}Si MAS NMR spectra were recorded for the pellets sintered at different temperatures by a solid state 400 MHz NMR spectrometer (Bruker AVANCE 400, Bruker Science (Biospin)), equipped with a 7 mm MAS probe, with a resonance frequency of 79.46 MHz for ^{29}Si nuclei. All ^{29}Si MAS NMR spectra were obtained with a 4 μs 90° pulse, a recycle delay of 10 s, and a sample spin-rate of 7 kHz. The ^{29}Si chemical shift was externally referenced to tetramethylsilane at 0.0 ppm.

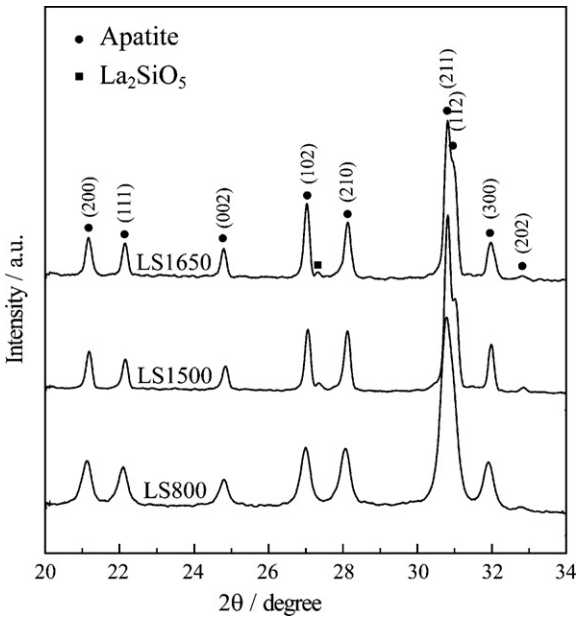

Fig. 1. X-ray diffraction patterns of the $La_{10}Si_6O_{27}$ calcined nanopowders at 800 °C (LS800), and sintered pellets at 1500 °C for 4 h (LS1500) and 1650 °C for 2 h (LS1650).

The micro-Raman spectra were recorded for the pellets sintered at different temperatures by a high-resolution dispersive Raman microscope (LabRAM HR UV/Vis/NIR, Horiba Jobin Yvon) equipped with three laser sources (UV, Vis, and NIR), a confocal microscope, and a liquid nitrogen cooled charge-coupled device (CCD) multichannel detector (256 pixels × 1024 pixels). The measurement was performed with a 514.5 nm line of an argon ion laser at room temperature. The laser power from the source is around 40 mW after passing through filtering optics and a microscope objective. A 50× objective lens was used and the acquisition time for each Raman spectrum was approximately 3 min depending on the sample. The Raman shift range acquired was from 100 to 1000 cm^{-1}.

3. Results and discussion

3.1. Phase and microstructural analysis

The XRD patterns of the $La_{10}Si_6O_{27}$ powder calcined at 800 °C and the fine ground powders of the pellets sintered at 1500 and 1650 °C are shown in Fig. 1. The patterns of the calcined powder and sintered pellets showed the single-phase, high degree of crystallinity of the $La_{10}Si_6O_{27}$ composition with a hexagonal apatite-type structure (space group $P6_3/m$). The sintered pellets contain small traces of La_2SiO_5 as an impurity phase regardless of their sintering temperatures. The XRD patterns of $La_{10}Si_6O_{27}$ samples are in agreement with JCPDS data # 53-0291. Table 1 presents the comprehensive lattice parameters of the $La_{10}Si_6O_{27}$ calcined powder and pellets sintered at different temperatures, and those

Table 1
Cell parameters of $La_{10}Si_6O_{27}$ powder calcined at 800 °C and pellets sintered at 1500 and 1650 °C.

Sample	Lattice parameters (Å)		Lattice volume (Å^3)
	a, *b*	*c*	
LS800	9.71 (±0.01)	7.18 (±0.01)	585.70
LS1500	9.68 (±0.01)	7.16 (±0.01)	581.61
LS1650	9.69 (±0.01)	7.17 (±0.01)	582.49

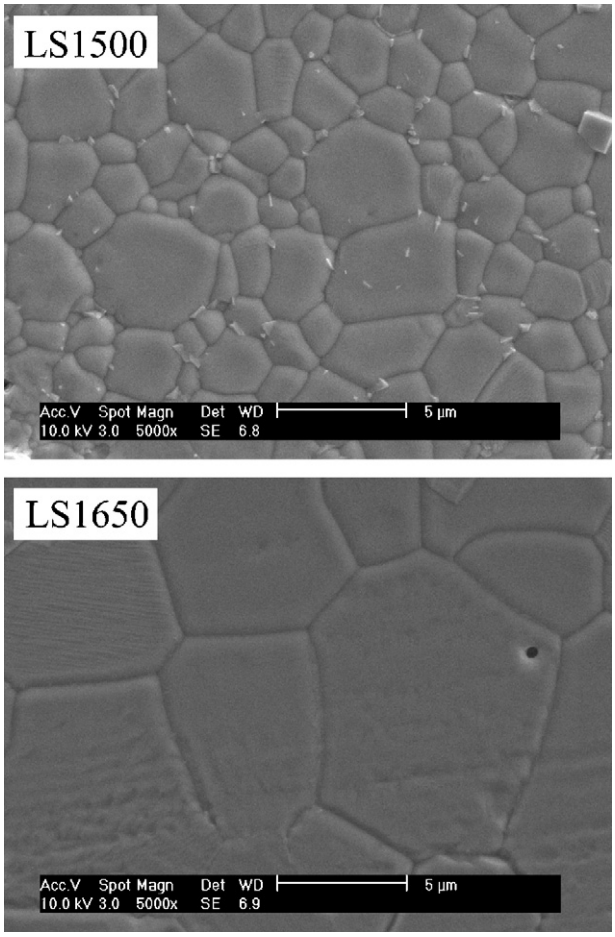

Fig. 2. SEM images of the polished and thermally etched surfaces of the $La_{10}Si_6O_{27}$ pellets.

are similar with the literature reports. Thus, the nanopowder synthesized via the DEA process showed a single-phase of $La_{10}Si_6O_{27}$ that was formed at a lower calcination temperature of 800 °C compared with solid state reaction. Fig. 2 shows the SEM images of the polished and thermally etched surfaces of the LS1500 and LS1650 pellets. The micrograph images of sintered pellets revealed the highly dense morphologies with negligible porosity, and clearly resolved grain boundaries, which are typical microstructural features of highly sintered pellets. The average size of grains in the sintered pellets LS1500 and LS1650 are 2.6 (±1.1) and 8.7 (±2.7) μm, respectively.

3.2. Electrical conductivity

Fig. 3a and b show the normalized complex impedance spectra with the sample geometry for the $La_{10}Si_6O_{27}$ pellet sintered at 1500 °C (LS1500), measured at 350 and 600 °C, respectively. The spectra for the pellet sintered at 1650 °C (LS1650), measured at 350 and 600 °C, are shown in Fig. 3c and d, respectively. Also Fig. 3a–d show the fit data and the schematic plots identifying the grain bulk, grain boundary and electrode regions. The presence of a depressed semicircle at a high-frequency range in Fig. 3a and c is probably due to the resistivity of a small grain bulk (R_b). The dominant large depressed semicircle in the middle-frequency region is due to the resistivity of a grain boundary (R_{gb}) response. The low-frequency region of the spectra may be attributed to electrode resistivity (R_{elect}). The impedance spectra measured at 600 °C exhibit only one depressed semicircle due to the grain boundary response and the low-frequency spectra due to the electrode. It can be clearly observed that the semicircles in the spectra shift to higher frequencies with increasing temperature. The detailed analyses of the impedance spectra with an equivalent circuit model are described in our previous reports [10,17]. The impedance behaviors of LS1500 and LS1650 were found to be similar in the measured temperature range. Therefore, possibly it can be concluded that the same oxide-ion conduction mechanism is involved for the different temperature sintered pellets.

The total resistivity (R_t) was obtained by fitting the impedance data with an equivalent circuit model using the nonlinear least-squares fitting program of the *Z-view* software. The total resistivity of the electrolyte is shown by $R_t = (R_b) + (R_{gb})$. Accordingly, the total electrical conductivity (σ_t) was calculated using pellets' dimensions and R_t of the samples. Fig. 4a shows the calculated total electrical conductivity as a function of temperature following the Arrhenius law in the following equation:

$$\sigma = \left(\frac{\sigma_o}{T}\right) \exp\left(-\frac{E_a}{RT}\right) \quad (1)$$

for the LS1500, LS1550, LS1600, and LS1650 pellets. The $La_{10}Si_6O_{27}$ pellet sintered at 1650 °C exhibited the ionic conductivity of 1.22×10^{-2} S cm^{-1} at 700 °C, which is similar to the value reported by Nakayama et al. for the pellet sintered at 1700 °C for 2 h (in Fig. 4a) [5]. The LS1650 pellet showed an increase in ionic conductivity by one order of magnitude compared with the pellets sintered at 1600 °C and below temperatures, which are produced from the same batch of nanopowder, as shown in Figs. 4a and b. Although, the sintered $La_{10}Si_6O_{27}$ pellet at 1650 °C showed quite enhanced electrical conductivity (Fig. 4b) but its activation energy (E_a) value was similar to those of the lower temperatures sintered pellets. This confirms that the LS1650 sample follows the same interstitial oxide-ion conduction mechanism of the $La_{10}Si_6O_{27}$ solid electrolytes as the sintered pellets below 1600 °C.

Table 2 represents the density, grain size and the calculated grain bulk, grain boundary and the total electrical conductivity of the pellets sintered at different temperatures. The observed negligible porosity for the different temperatures sintered samples confirms the insignificant contribution of the porosity on the ionic conductivity. Also, the slight variation in grain sizes for the LS1600 and LS1650 pellets may not be the major factors to control their large difference in ionic conductivity. Therefore, the observed increase in the total ionic conductivity for LS1650 compared to lower temperatures sintered pellets (LS1500, LS1550 and LS1600) can be attributed to the combined contributions of bulk and grain boundary conductivities. The trace amount of secondary La_2SiO_5 impurity phase was confirmed from the XRD investigation (Fig. 1) regardless of their sintering temperatures. Even though the segregated impurity phase at the grain boundary influences on the total ionic conductivity for the different temperatures (1500–1650 °C) sintered pellets, but still there is observed increase in the conductivity for the LS1650 pellet. This enhancement of total conductivity for LS1650 can be attributed to the combined contributions of bulk and grain boundary conductivities through structural changes facilitating high ionic conduction pathways. Recently, Martínez-González et al. [20] reported that the observed large difference in the ionic conductivity, and similarity in the activation energy for the $La_{10}Si_6O_{27}$ electrolytes synthesized from amorphous silica and crystalline SiO_2 was explained based on the degree of structural distortion. Therefore, the predictable explanation for the increased ionic conductivity of the high temperature sintered LS1650 pellet may be attributing to the formation of a beneficial local structural distortion, which is thermodynamically stabilized at elevated temperature as a result of the silicate substructure that can lead to better conduction pathways. Thus, the significant increase in conductivity of the pellet sintered at 1650 °C (LS1650) is possibly

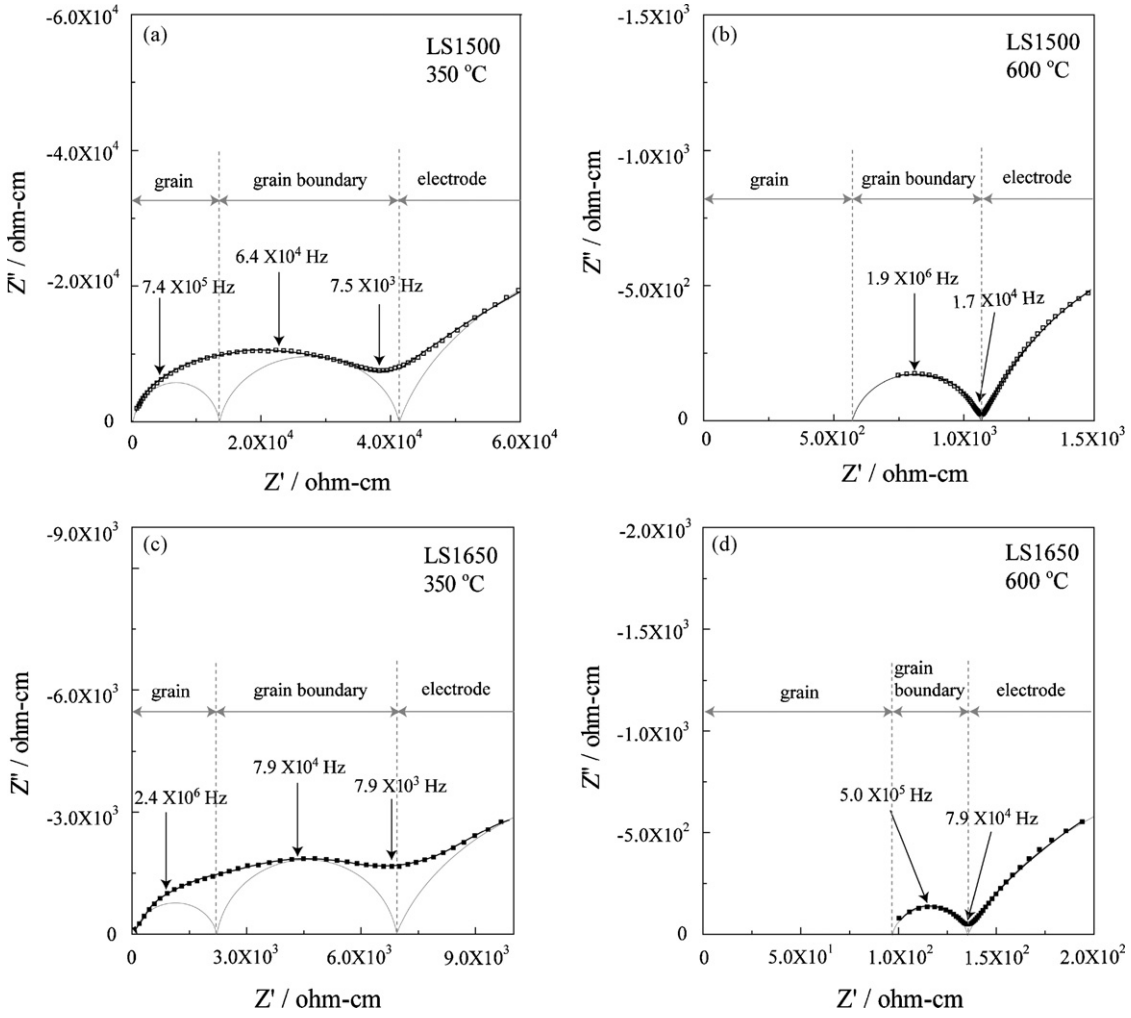

Fig. 3. Impedance spectra of LS1500, measured at (a) 350 °C and (b) 600 °C, and LS1650, measured at (c) 350 °C and (d) 600 °C.

explained with the support of characterization techniques including the Raman and ^{29}Si NMR spectroscopic results.

3.3. ^{29}Si MAS NMR and Raman studies

A typical ^{29}Si MAS NMR spectrum is shown in Fig. 5 for the $La_{10}Si_6O_{27}$ pellet sintered at 1500 °C for 4 h, which is consistent with the literature reports [17,18]. An intense peak at a chemical shift of −77.5 ppm can be assigned to isolated tetrahedral $[SiO_4]^{4-}$ units. The observed weak peak at −81.2 ppm can be attributed to a $[SiO_4]^{4-}$ unit adjacent to an interstitial oxide-ion site, which represents a pseudo-"SiO_5" unit [17,18]. In addition, another weak peak at a lower chemical shift of −85.0 ppm corresponds to condensation of two $[SiO_4]^{4-}$ units to form $[Si_2O_7]^{6-}$ units. It is recognized in the apatite-structure that the effect of such condensation of $[SiO_4]^{4-}$ units will be the creation of additional interstitial oxide-ion defects, i.e. $2[SiO_4]^{4-} = [Si_2O_7]^{6-} + O_{int}^{2-}$ [18]. As a result the NMR data confirmed the presence of silicate groups adjacent to interstitial oxygen sites in apatite materials sintered at 1500–1650 °C, which are important in the conduction process [17,18,21]. But there was no clear evidences from the ^{29}Si NMR spectra for the difference of approximately one order of increase in conductivity of the LS1650 pellet sintered at 1650 °C compared with the values for the pellets sintered at lower temperatures.

The Raman spectra for the LS1500, LS1550, LS1600 and LS1650 samples in the ranges from 100 to 1000 cm^{-1} are shown in Fig. 6.

Table 2
The density, grain size and the calculated grain bulk (σ_b), grain boundary (σ_{gb}) and the total electrical conductivities (σ_t), measured at 600 and 650 °C, of the $La_{10}Si_6O_{27}$ pellets sintered at different temperatures.

Sample	Relative density (%)	Grain size (μm)	Measure temperature (°C)	σ_b (S cm^{-1})	σ_{gb} (S cm^{-1})	σ_t (S cm^{-1})
LS1500	94.7 (±0.1)	2.6 (±1.1)	600	1.82×10^{-3}	1.92×10^{-3}	9.34×10^{-4}
			650	2.08×10^{-3}	6.90×10^{-3}	1.59×10^{-3}
LS1550	95.5 (±0.1)	3.9 (±0.9)	600	1.54×10^{-3}	2.80×10^{-3}	9.95×10^{-4}
			650	1.81×10^{-3}	1.15×10^{-2}	1.56×10^{-3}
LS1600	97.2 (±0.1)	6.3 (±1.8)	600	2.92×10^{-3}	1.32×10^{-3}	9.10×10^{-4}
			650	2.46×10^{-3}	3.88×10^{-2}	1.51×10^{-3}
LS1650	96.5 (±0.1)	8.7 (±2.7)	600	7.62×10^{-3}	1.64×10^{-2}	5.20×10^{-3}
			650	9.42×10^{-3}	7.82×10^{-2}	8.40×10^{-3}

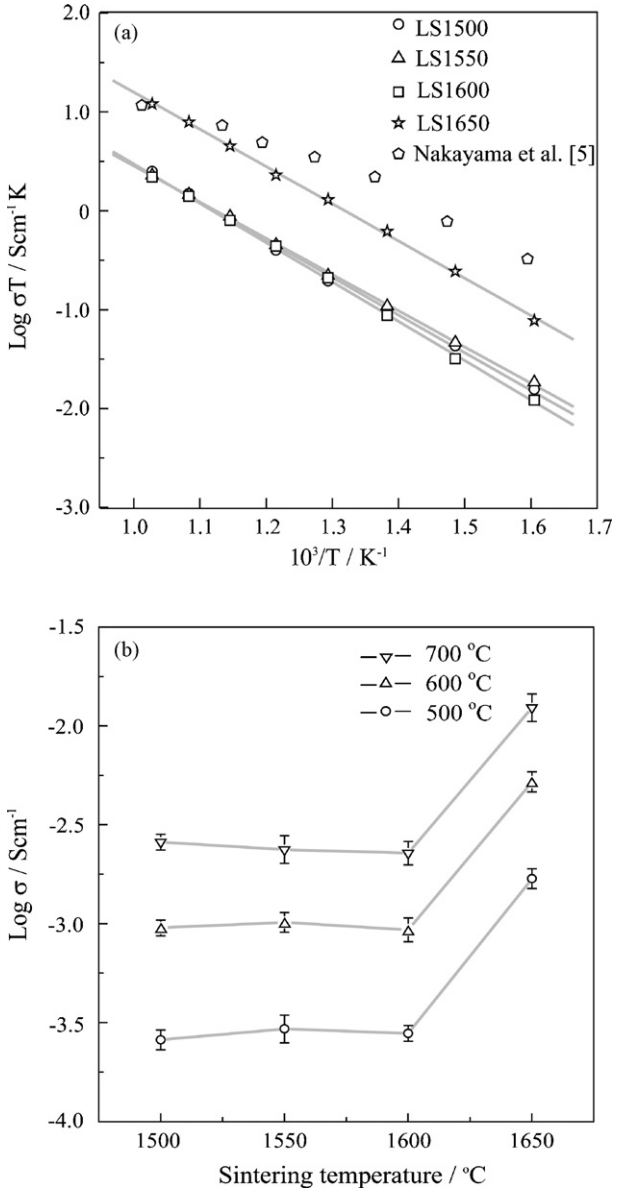

Fig. 4. Total electrical conductivity versus 1000/T plots of the $La_{10}Si_6O_{27}$ pellets sintered at various temperatures compared with Nakayama et al. report sintered at 1700 °C.

The observed major bands positions were assigned to their corresponding modes based on the related apatite-structured samples in the literature reports, including $La_{8+x}Sr_{2-x}(SiO_4)_6O_{2+x/2}$ [17], $La_{10-x}(SiO_4)_6O_{3-1.5x}$ [22] and $La_{10-x}(SiO_4)_6(AlO_4)_yO_{2+\delta}$ [23]. The peak above 350 cm^{-1} range is assigned to internal modes of pseudo-tetrahedral SiO_4 units at frequencies closely related to those of free species [17]. The Raman spectra for the different temperatures sintered pellets showed two major intense bands centered at 853 and 383 cm^{-1}. The intense band at 853 cm^{-1} can be assigned to the symmetric stretching mode ν_1 of SiO_4 tetrahedra [23]. The weak band at 978 cm^{-1} can be attributed to the asymmetric stretching mode ν_3. Another intense band at 383 cm^{-1} assigned to the symmetric bending mode ν_2 of the SiO_4 group and 523 cm^{-1} to the asymmetric bending mode ν_4.

The Raman stretching modes are specifically sensitive to the neighboring disorders (particularly atoms from other sub-lattices or electric defects resulting from substitutions/vacancies) and symmetric bending band modes to local geometric disorientation [24]. Thus, it should be convenient to observe the change in symmetric

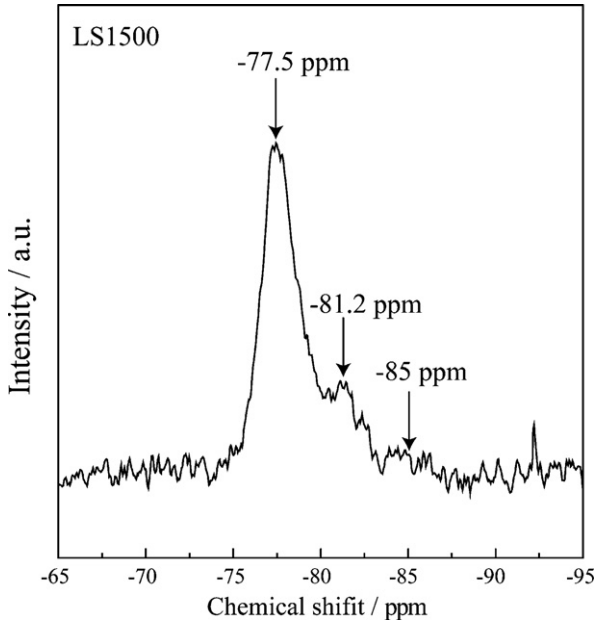

Fig. 5. ^{29}Si NMR spectrum for LS1500, measured at room temperature.

stretching mode ν_1 of SiO_4 tetrahedra to discriminate the neighboring disorder related to oxygen defects in $La_{10}Si_6O_{27}$ samples to evaluate the difference in conductivity of different temperatures sintered pellets.

Fig. 7a and b show for the LS1500 and LS1650 pellets the Lorentzian fit spectra of the specific symmetric stretching mode ν_1 band decomposed to three main bands at 845, 853 and 861 cm^{-1}, respectively. In Fig. 7a and b, the intensity of a new band at 861 cm^{-1} is lower for the 1500 °C sintered pellet compared with the pellet sintered at 1650 °C. It is evident from the decomposed spectral bands using Lorentzian fit that the relative intensity of each band differs with the sintering temperatures. The splitting of the ν_1 Raman mode at 861 cm^{-1} band with enhanced intensity may be possibly explained based on the lowered symmetry of the silicate group due to a strong distortion at a critical sinter-

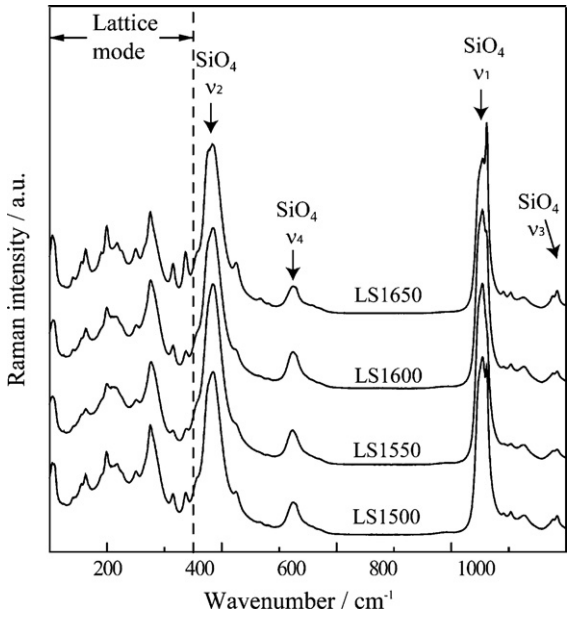

Fig. 6. Raman spectra for the $La_{10}Si_6O_{27}$ pellets sintered at different temperatures, measured at room temperature.

Table 3
The composition, total electrical conductivity (σ_t) at 700 °C and activation energy (E_a) obtained for the $La_{10}Si_6O_{27}$ pellets synthesized via different methods followed by sintering at different temperatures.

Sample/composition	Synthesis process	Sintering condition	σ_t (S cm^{-1}) at 700 °C	E_a (eV)	Ref.
$La_{9.55}Si_6O_{26.32}$	Solid state reaction	1300 °C for 24 h	$\sim 3.1 \times 10^{-4}$	0.88	[13]
$La_{10}Si_6O_{27}$	DEA precipitation	1400 °C for 10 h	$\sim 2.5 \times 10^{-3}$	0.68 (±0.01)	[10]
$La_{10}Si_6O_{27}$	Sol–gel process	1400 °C for 20 h	$\sim 1.9 \times 10^{-3}$	0.65 (±0.1)	[11]
$La_{10}Si_6O_{27}$	DEA precipitation	1500 °C for 4 h	2.33×10^{-3}	0.66 (±0.02)	Present study
$La_{9.6}Si_6O_{26.4}$	Solid state reaction	1500 °C for 3 h	$\sim 8.1 \times 10^{-4}$	-	[20]
$La_{10}Si_6O_{27}$	Freeze drying	1500 °C for 0 h	1.39×10^{-3}	0.83 (5)	[26]
$La_{10}Si_6O_{27}$	Gel-casting	1550 °C for 4 h	$\sim 2.8 \times 10^{-3}$	0.91	[27]
$La_{10}Si_6O_{27}$	DEA precipitation	1600 °C for 4 h	2.23×10^{-3}	0.72 (±0.01)	Present study
$La_{10}Si_6O_{27}$	DEA precipitation	1650 °C for 2 h	1.22×10^{-2}	0.68 (±0.01)	Present study
$La_{10}Si_6O_{27}$	Gel-casting	1650 °C for 4 h	$\sim 1.8 \times 10^{-2}$	0.77	[27]
$La_{10}Si_6O_{27}$	Solid state reaction	1700 °C for 2 h	$\sim 1.2 \times 10^{-2}$	0.64	[5]
$La_{10}Si_6O_{27}$	Solid state reaction	1700 °C for 10 h	$\sim 1.6 \times 10^{-2}$	0.62	[28]

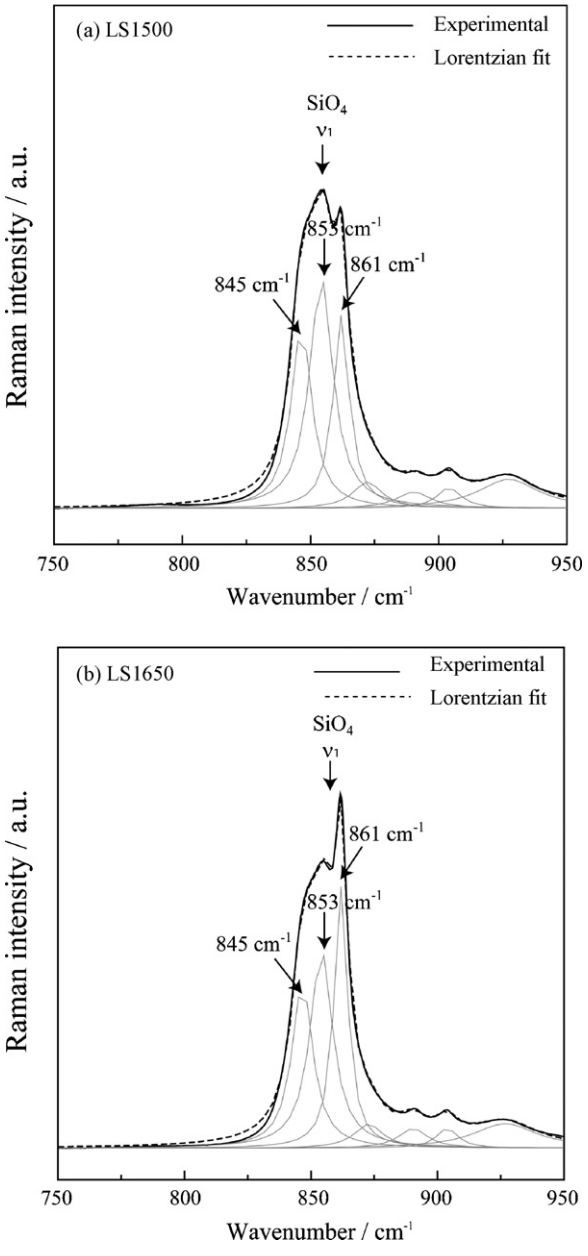

Fig. 7. Decomposition of the symmetric stretching mode ν_1 of SiO_4 tetrahedra into Lorentzian components for (a) LS1500 and (b) LS1650 samples.

ing temperature. Jones et al. have reported that interstitial oxygen is passed from one silicate unit to an adjacent unit involving a stage where it is coordinated to two SiO_4 units, resulting in the formation of a larger "Si_2O_9" unit [16,25]. Thus, the conduction process is aided by co-operative relaxation of the silicate substructures suggesting that the additional interstitial oxide-ion is passed from one silicate unit to another, which is essential to facilitate the high oxide-ion conductivity for the pellet sintered at 1650 °C. This result relates with the high thermal displacement parameters for the silicate oxygen atoms observed in Raman studies, particularly for the stretching mode of SiO_4 groups with the oxide-ion channels. Thus, approximately one order of increased conductivity for LS1650 compared with the sintered pellets at lower temperatures can be possibly explained through the additional interstitial ions conduction pathways created by the local structural distortions near oxide-ion interstitial sites, which were identified from the new Raman band attributed to stretching mode at 861 cm^{-1} of SiO_4 unit. This shows that the local relaxation around the interstitial sites leads to reduction in the distance to a neighboring SiO_4 unit and possibly creates an effective conduction pathway, as Kendrick et al. reported that an interstitial oxide-ion is moved between adjacent channels by a series of two co-operative processes of rotation for the tetrahedral of SiO_4 units [16].

Table 3 represents consolidated ionic conductivity data obtained from different temperatures sintered lanthanum silicate samples fabricated from various powder processing methods [5,10,11,13,20,26–28]. In the literature, it is evidently confirmed that the wet chemical method synthesized powders can form a pure crystalline phase at lower calcination temperature, such as 800 °C. In addition using such a nanopowder, it is possible to produce highly densified pellets at lower sintering temperatures such as 1400 °C and above. But, the ionic conductivities exhibited by those pellets are approximately one order of magnitude lower compared with pellets sintered above 1600 °C, which shows a similar conductivity behavior as reported in the present results. Therefore, at this moment it is concluded that the sintering temperature for the $La_{10}Si_6O_{27}$ apatite-type materials is crucial parameter to obtain high oxide-ion conductivity and this sintering temperature needs to be above 1600 °C.

4. Conclusions

Dense apatite-type structure $La_{10}Si_6O_{27}$ pellets were successfully fabricated using nanopowder synthesized via the DEA process followed by different sintering temperatures from 1500 to 1650 °C. The impedance spectroscopy results demonstrated the influence of the sintering temperatures on the ionic conductivity of the $La_{10}Si_6O_{27}$ electrolytes. The $La_{10}Si_6O_{27}$ pellet sintered at 1650 °C (LS1650) revealed a higher ionic conductivity (1.22×10^{-2} S cm^{-1} at 700 °C) of approximately one order of magnitude than the

pellets sintered at lower temperatures. The ^{29}Si NMR data confirmed the presence of interstitial oxygen sites that contribute to oxide-ion conduction. The Raman peaks revealed the appearance of a resolved new mode centered at 861 cm^{-1} and confirmed the possibility of local structural distortions near oxide-ion interstitial sites at the sintering temperature above 1600 °C. Thus, the conduction pathway may be determined by the co-operative relaxation of the SiO_4 substructure units formed at elevated sintering temperature for high oxide-ion conductivity. Therefore, the present work concludes that the high ionic conductivity of $La_{10}Si_6O_{27}$ apatite-structured materials can be achieved mainly by sintering the pellets above 1600 °C, in addition with the characteristics of pure single-phase, high densification.

Acknowledgments

This work was financially supported by the Korea Research Foundation Grant funded by the Korean government (MOEHRD; KRF-2008-005-J00903). This work was also partially supported by Brain Korea 21 (BK21) program from Korean Ministry of Education.

References

[1] T. Ishihara, H. Matsuda, Y. Takita, J. Am. Chem. Soc. 116 (1994) 3801.
[2] D.R. Ou, T. Mori, F. Ye, M. Takahashi, J. Zou, J. Drennan, Acta Mater. 54 (2006) 3737.
[3] W. Jung, J.L. Hertz, H.L. Tuller, Acta Mater. 57 (2009) 1399.
[4] S.H. Jo, P. Muralidharan, D.K. Kim, Solid State Ionics 178 (2008) 1990.
[5] S. Nakayama, M. Sakamoto, J. Eur. Ceram. Soc. 18 (1998) 1413.
[6] S. Nakayama, M. Sakamoto, M. Higuchi, K. Kodaira, M. Sato, S. Kakita, T. Suzuki, K. Itoh, J. Eur. Ceram. Soc. 19 (1999) 507.
[7] H. Arikawa, H. Nishiguchi, T. Ishihara, Y. Takita, Solid State Ionics 136 (2000) 31.
[8] A.L. Shaula, V.V. Kharton, F.M.B. Marques, Solid State Ionics 177 (2006) 1725.
[9] Y.V. Pivak, V.V. Kharton, A.A. Yaremchenko, S.O. Yakovlev, A.V. Kovalevsky, J.R. Frade, F.M.B. Marques, J. Eur. Ceram. Soc. 27 (2007) 2445.
[10] S.H. Jo, P. Muralidharan, D.K. Kim, J. Mater. Res. 24 (2008) 237.
[11] S.W. Tao, J.T.S. Irvine, Mater. Res. Bull. 36 (2001) 1245.
[12] C. Tian, J. Liu, J. Cai, Y. Zeng, J. Alloys Compd. 458 (2008) 378.
[13] L. Leon-Reina, E.R. Losilla, M. Martinez-Lara, S. Bruque, M.A.G. Aranda, J. Mater. Chem. 14 (2004) 1142.
[14] P.R. Slater, J.E.H. Sansam, Solid State Chem. V 90–91 (2003) 195.
[15] J.R. Tolchard, M.S. Islam, P.R. Slater, J. Mater. Chem. 13 (2003) 1956.
[16] E. Kendrick, M.S. Islam, P.R. Slater, J. Mater. Chem. 17 (2007) 3104.
[17] A. Orera, E. Kendrick, D.C. Apperley, V.M. Orera, P.R. Slater, Dalton Trans. (2008) 5296.
[18] J.E.H. Sansom, J.R. Tolchard, M.S. Islam, D. Apperley, P.R. Slater, J. Mater. Chem. 16 (2006) 1410.
[19] P. Muralidharan, S.H. Jo, D.K. Kim, J. Am. Ceram. Soc. 91 (2008) 3267.
[20] L.G. Martínez-González, E. Rodríguez-Reyna, K.J. Moreno, J.I. Escalante-García, A.F. Fuentes, J. Alloys Compd. 476 (2009) 710.
[21] E. Kendrick, D. Headspith, A. Orera, D.C. Apperley, R.I. Smith, M.G. Francesconi, P.R. Slater, J. Mater. Chem. 19 (2009) 749.
[22] E. Rodríguez-Reyna, A.F. Fuentes, M. Maczka, J. Hanuza, K. Boulahya, U. Amador, J. Solid State Chem. 179 (2006) 522.
[23] G. Lucazeau, N. Sergent, T. Pagnier, A. Shaula, V. Kharton, F.M.B. Marques, J. Raman Spectrosc. 38 (2007) 21.
[24] G. Gouadec, P. Colomban, Prog. Cryst. Growth Charact. Mater. 53 (2007) 1.
[25] A. Jones, P.R. Slater, M.S. Islam, Chem. Mater. 20 (2008) 5055.
[26] A. Chesnaud, G. Dezanneau, C. Estournes, C. Bogicevic, F. Karolak, S. Geiger, G. Geneste, Solid State Ionics 179 (2008) 1929.
[27] S.P. Jiang, L. Zhang, H.Q. He, R.K. Yap, Y. Xiang, J. Power Sources 189 (2009) 972.
[28] A. Mineshige, T. Nakao, M. Kobune, T. Yazawa, H. Yoshioka, Solid State Ionics 179 (2008) 1009.